Laminated Amorphous Polymers Subjected to Low-Velocity Impacts

Andreas Rühl[1], Stefan Kolling[2], Jens Schneider[2], Bernd Kiesewetter[3]

[1]TH Mittelhessen, Wiesenstraße 14, 35390 Gießen, Germany
[2]TU Darmstadt, Franziska-Braun-Straße 3, 64287 Darmstadt, Germany
[2]Evonik Industries AG, Kirschenallee, 64293 Darmstadt, Germany

1 Introduction

Weight reduction is one of the most important aims in the development and design of vehicles. Today's car light housings are already composed of amorphous (glassy) polymers, like polycarbonate (PC) and poly(methyl methacrylate) (PMMA). In particular, PMMA shows very good optical properties, weatherability, and its brittleness makes its behavior similar to that of conventional mineral glass. However, the clear majority of today's car windows are still made of conventional toughened safety glass (TSG) or laminated safety glass (LSG). A direct substitution of TSG with monolithic PMMA exhibits post-breakage disadvantages due to bigger fragments because of the special heat treatment of TSG. Nevertheless, PMMA can be combined with a highly elastic interlayer material, like poly(vinyl butyral) (PVB) or thermoplastic polyurethane (TPU), to form a laminated structure. The resulting laminate combines the advantageous properties of PMMA with a high deformation and post-breakage capacity as well as an improved fracture behavior.

Laminated PMMA structures with a thickness of a few millimeters and in combination with PC or glass were subject to investigation so far, see [1], [2] and [3]. A further huge field of research is focused on laminated safety glass, which is the standard application for automotive windscreens [4], [5] and for safety applications in civil engineering [6]. A laminate consisting exclusively of PMMA in combination with a TPU interlayer was introduced in [7] and is currently subject to further research and development [8]. The homogeneous structure of PMMA-TPU-PMMA, as shown in Figure 1, bears the advantage of equally distributed coefficients of thermal expansion, which reduces the internal thermal stress. The laminate has superior acoustic properties and it passes the UNECE regulation 43 [7]. Furthermore, the superior UV- and weatherability as well as scratch resistance of PMMA compared to PC reduces the need of treatment with additional coatings.

Due to the recent development of this laminate, an experimental data basis as well as computational prediction methods are required to increase the acceptance and usage within the industrial environment. The aim of the present work is the creation of an experimental basis to identify and to characterize the principle behavior of the laminate. Furthermore, FE modelling and a suitable material law have to be found, which are able to represent the setup of the laminated structure as well as its time and temperature dependent behavior.

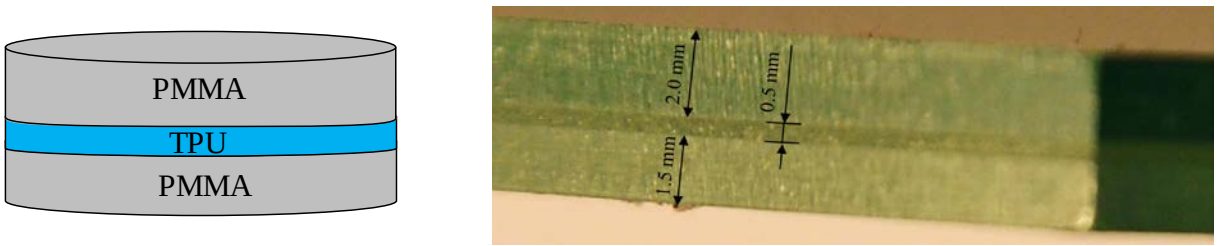

Figure 1 – PMMA-TPU-PMMA laminate: The left-hand side shows the setup of the laminate in principle. The right hand-side shows a detail of the specimens used in this study. As for dimensioning, the 2.0mm upper side is subjected to loading.

2 Experimental Basis

2.1 PMMA

For a basic characterization, PMMA was subjected to uniaxial tensile tests as well as Dynamic Mechanical Thermal Analyses (DMTA) in a three-point bending setup. The stress-strain correlation at different velocities is shown in Figure 2 (left) and exhibits a rate-dependent behavior and a brittle failure at small strains. The corresponding strain rates are approximately 10^{-4} 1/s (1.0 mm/min), 10^{0}1/s (0.1 m/s) and 10^{2} 1/s (3.0 m/s). A master curve was obtained from DMTA results to describe the material for a wide range of frequencies with the help of the time-temperature superposition. This master curve is shown in Figure 2 (right) and was used for determining the viscoelastic parameters of the material. The thermomechanical behavior is proved to follow the Arrhenius shift approach

$$\log a_T(T,T_{\text{ref}}) = \frac{0.43E_A}{R}\left(\frac{1}{T}-\frac{1}{T_{\text{ref}}}\right) \tag{1}$$

for temperatures up to 60°C. Here, a_T is the shift factor, E_A the activation energy, R the universal gas constant, T the temperature and T_{ref} a corresponding reference temperature.

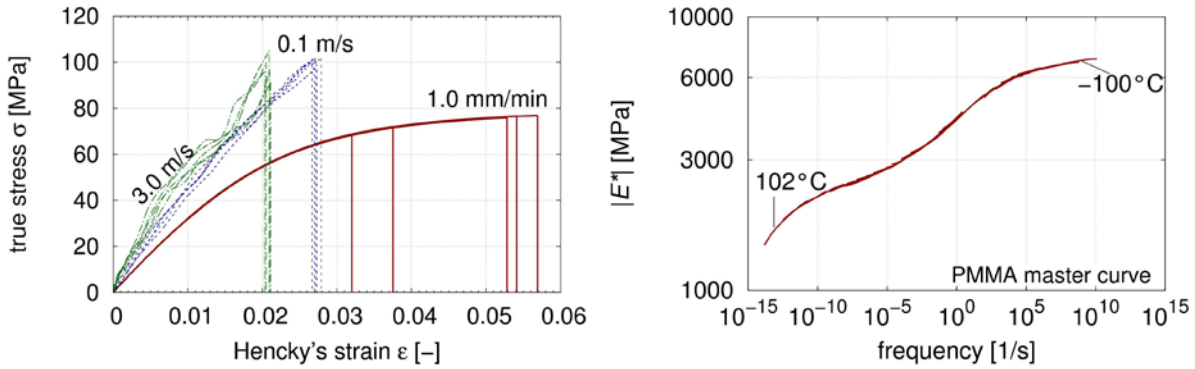

Figure 2 – Dynamic uniaxial tensile tests with PMMA (left) and master curve determined from DMTA experiments (right).

2.2 TPU

TPU was subjected to uniaxial tensile tests at different velocities as well as DMTA in shearing setup. The corresponding stress-strain relation for different experiment velocities are shown in Figure 3 (left). The initial strain rates of the tests are approximately 10^{-3} 1/s (5.0 mm/min), 10^{0} 1/s (0.1 m/s), and 10^{2} 1/s (3.0 m/s). Due to the high stretch of the material the true strain rate showed to decrease by one decade over the whole test range. The material exhibited as highly elastic with a significant dependency on the strain rate.

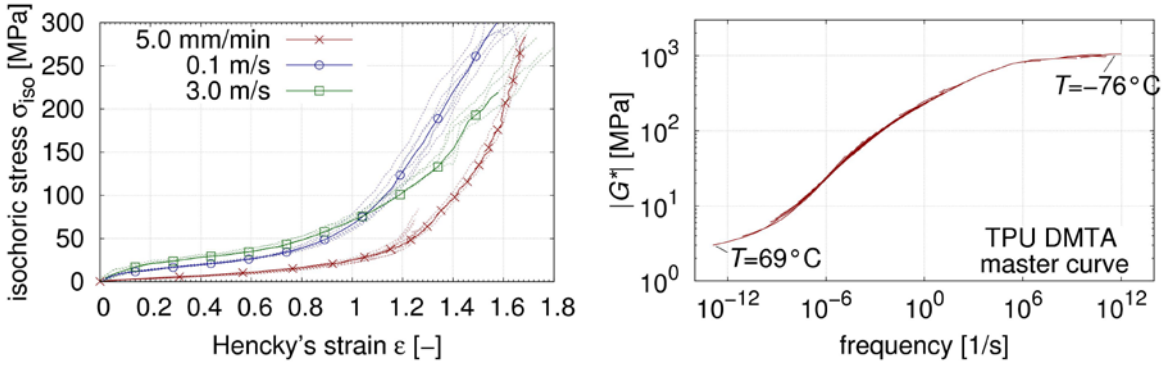

Figure 3 – Dynamic uniaxial tensile tests with TPU (left) and master curve determined from DMTA experiments (right).

The stress-strain curves of the experiments at 0.1m/s and 3.0m/s show a reproducible crossing at approximately 100% true strain, which may be caused by quasi-adiabatic heating of the material. Temperature measurements with an infrared thermal camera revealed temperature rises of at least 10K, which has a significant influence on the mechanical behavior near the glass transition. For a temperature range between -80°C and 50°C and under the assumption of a thermorheologically simple material behavior the thermomechanical material behavior was described well with the Williams-Landel-Ferry (WLF) shift equation [9] following

$$\log a_T(T, T_{\text{ref}}) = -\frac{C_1(T - T_{\text{ref}})}{C_2 + T - T_{\text{ref}}}, \tag{2}$$

where C_1 and C_2 are material parameters.

2.3 PMMA-TPU Laminate

2.3.1 Mechanical Behavior

In order to characterize the mechanical behavior of the material, dart impact tests were conducted at 5.0 m/s. Hereby, the used laminated disc specimen that were positioned freely on a cylindrical support with an inner diameter of d=70mm. The experimental setup is shown in Figure 4. The behavior is characterized by an initial rise of force until failure of the PMMA plies. After that the post-breakage phase begins, which enables the laminate to absorb huge additional impact energy. Furthermore, splinters are prevented to break loose, which reduces the injury risk and objects are more likely be prevented to penetrate the due to the highly elastic interlayer.

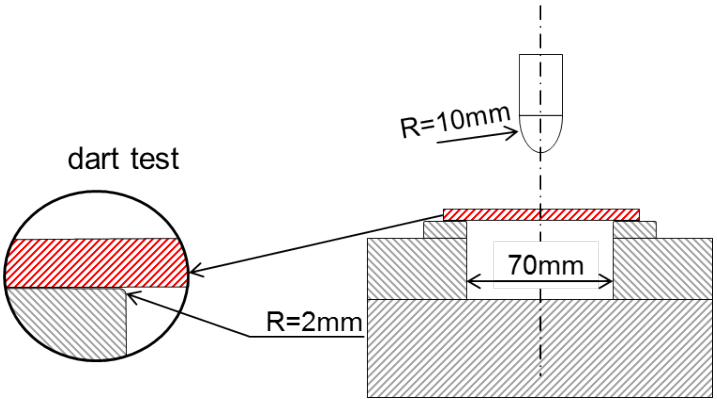

Figure 4 – Experimental setup for dart impact test.

2.3.2 Temperature Dependency

In a further test series, the dart test was conducted at temperatures of -30°C, 0°C, 22°C and 60°C at 5.0 m/s in order to observe the temperature dependency of the material. The temperature exhibited to have a significant effect on the mechanical behavior of the laminate. At -30°C almost no post-breakage phase can be observed, which is mainly caused by the interlayer being in its glassy state. At 0°C and 22°C the interlayer shows to be more rubbery, which is the basis for the creation of a post-breakage phase. At 60°C, thermal softening becomes dominant, which leads to smaller maximum forces, and therefore less energy absorption. Summarizing, the laminate has a clear optimal temperature to absorb most energy, which is around room temperature. Below this temperature, the glass transition of the interlayer embrittles the whole laminate and above that temperature thermal softening effects become dominant.

3 Material Modeling

3.1 PMMA

The experiments revealed a strain-rate dependent behavior and small strains until failure with no major plasticity visible at a-posteriori specimen inspection. Therefore, modelling with a linear viscoelastic model, i.e. the generalized Maxwell model (*MAT_076), which is depicted in Figure 5, appears as a worthwhile approach for the tensile area of PMMA.

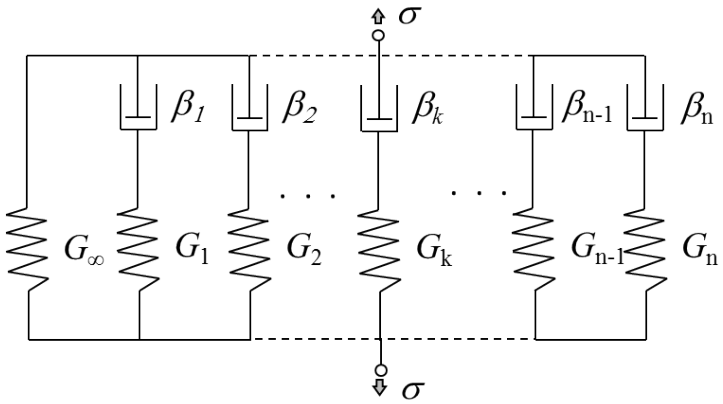

Figure 5 – Generalized Maxwell model.

The parameters for this model were obtained by using the master curve determined in the experimental section and comparing it to the model's master curve, which is governed by

$$G'(\omega) = G_\infty - \sum_{i=1}^{n} \frac{G_i \omega^2}{\beta_i^2 + \omega^2} \tag{3}$$

and

$$G''(\omega) = \sum_{i=1}^{n} \frac{G_i \omega}{\beta_i^2 + \omega^2 / \beta_i} . \tag{4}$$

Both material constants, the storage modulus *G'* and the loss modulus *G''* describe the complex modulus

$$G^*(\omega) = G' + iG'' \tag{5}$$

and the absolute value

$$|G^*(\omega)| = \sqrt{(G')^2 + (G'')^2} . \tag{6}$$

Here, for each decade in frequency roughly one Maxwell element (springer-damper coupling) is dominant, which allows the stepwise adjustment of the parameter set. With a total of $n = 17$ Maxwell elements and one infinite (time independent) spring it was possible to reproduce the master curve as well as the tensile test with the same parameter set.

3.2 TPU

TPU was modelled using the generalized Maxwell model from Figure 7, but with a hyperelastic infinite spring (*MAT_077H) governed by the polynomial

$$W(\bar{I}_C, \bar{II}_C, J) = C_{ij}(\bar{I}_C - 3)^i(\bar{II}_C - 3)^j + W_H(J), \tag{7}$$

where I_C and II_C are the first and seconding deviatoric invariants of the right Cauchy Green stress tensor, J the Jacobian determinant and C_{ij} are material parameters. The material parameters were determined using uniaxial tensile tests. The material model was capable to reproduce the uniaxial behavior of the material for different haul-off velocities and high strains.

4 Finite Element Modelling

The finite element model was set up under the assumption of perfect bonding between the plies, which enables a coincident node modelling as shown in Figure 6 (left). The thickness of the shell plies was given an offset in order to obtain a physical structure without smearing of the plies, i.e. overlapping of the shell thickness into the solid elements. A further advantage is a longer conservation of mass, which is lumped in the nodes and only deleted if both shell and solid elements are deleted. An unstructured element (Figure 6, right) structure exhibited a more realistic fracture pattern when working with a first principal stress failure criterion for element deletion. The first principal stress criterion was improved by using a nonlocal energy threshold introduced by [10] in order to capture the initial failure of the plies. All simulations were conducted with LS-DYNA v971 d R9.0.0 in SMP mode.

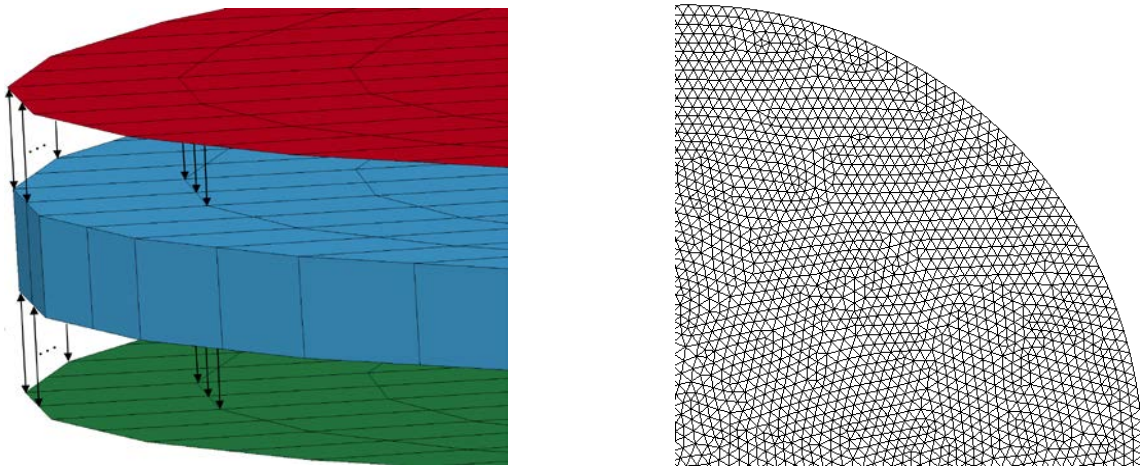

Figure 6 – Coincident model of the laminate (left) and unstructured mesh setup with triangular elements (right).

5 Simulation Results

For evaluating the material and FE models, dart tests at different temperatures and head impact tests on automotive side windows were conducted, which are depicted in Figure 7 as image series. The simulations were capable to predict the time and temperature dependent force-displacement behavior of the laminate for temperatures between -30°C and 60°C well for the most part, which is shown in Figure 8. Furthermore, the impact on a laminated side window was reproduced with high agreement in terms of force-displacement behavior and with principle agreement in terms of the fracture pattern using a first principal stress failure criterion. Due to the simplified failure criterion crack velocity is not represented correctly within this model. Here, methods like the XFEM [11] are promising approaches for further improvements.

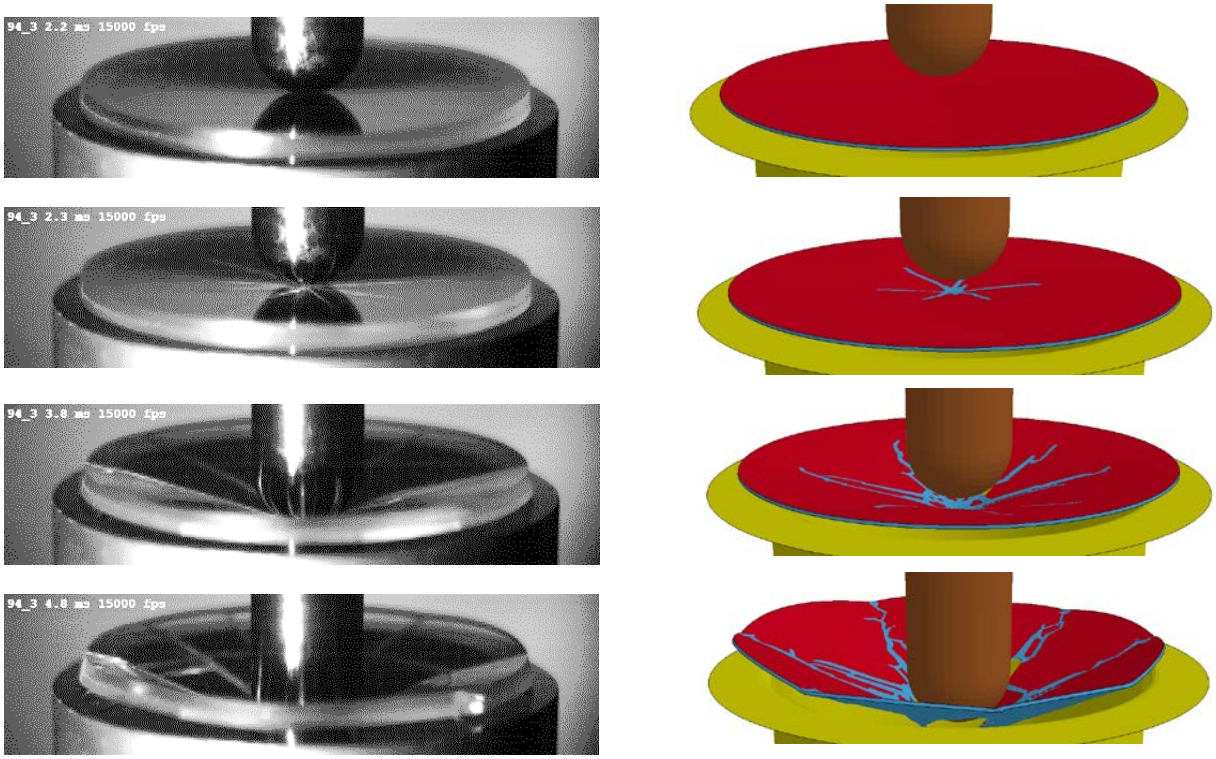

Figure 7 – Image series of the dart impact at 5 m/sand room temperature test compared to simulation results.

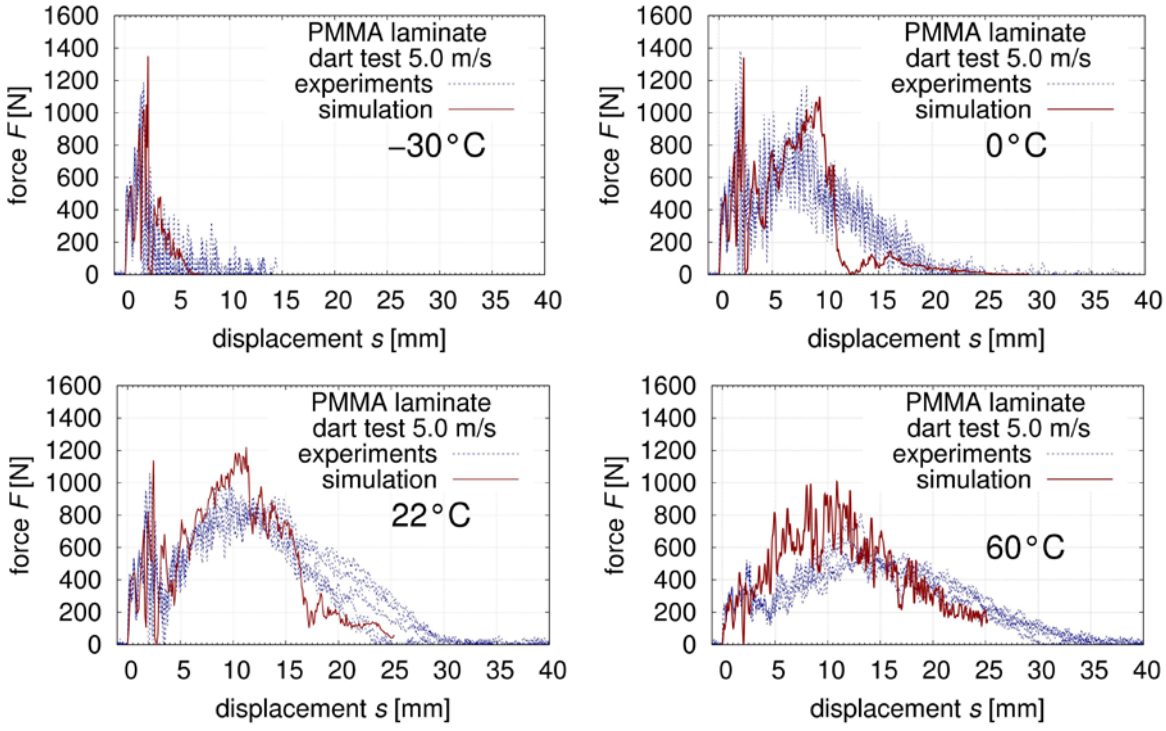

Figure 8 – Dart impact test on laminate at 5 m/s and different temperatures. Simulation and experiments in comparison.

6 Head Impact Test on Automotive Side Window

Early stages of the presented material models were used in [12] to simulate the head impact experiments consisting of a head dummy with a total mass of 3.5 kg, which impacts an automotive side window at 10 m/s. These experiments were calculated with the final models presented here and are briefly shown subsequently. The head impact dummy FE-model was kindly provided by LASSO Ingenieurgesellschaft mbH. Figure 9 depicts and image series of the experiment compared to numerical results while Figure 10 gives the final simulation model in comparison to two experiments. The overall agreement consisting of a correct representation of the initial stiffness, the failure, and the post-breakage behavior can be retrieved from Figure 9 and Figure 10. As Figure 9 indicates, the fracture pattern is highly influenced by the mesh structure and element type as well as the element size.

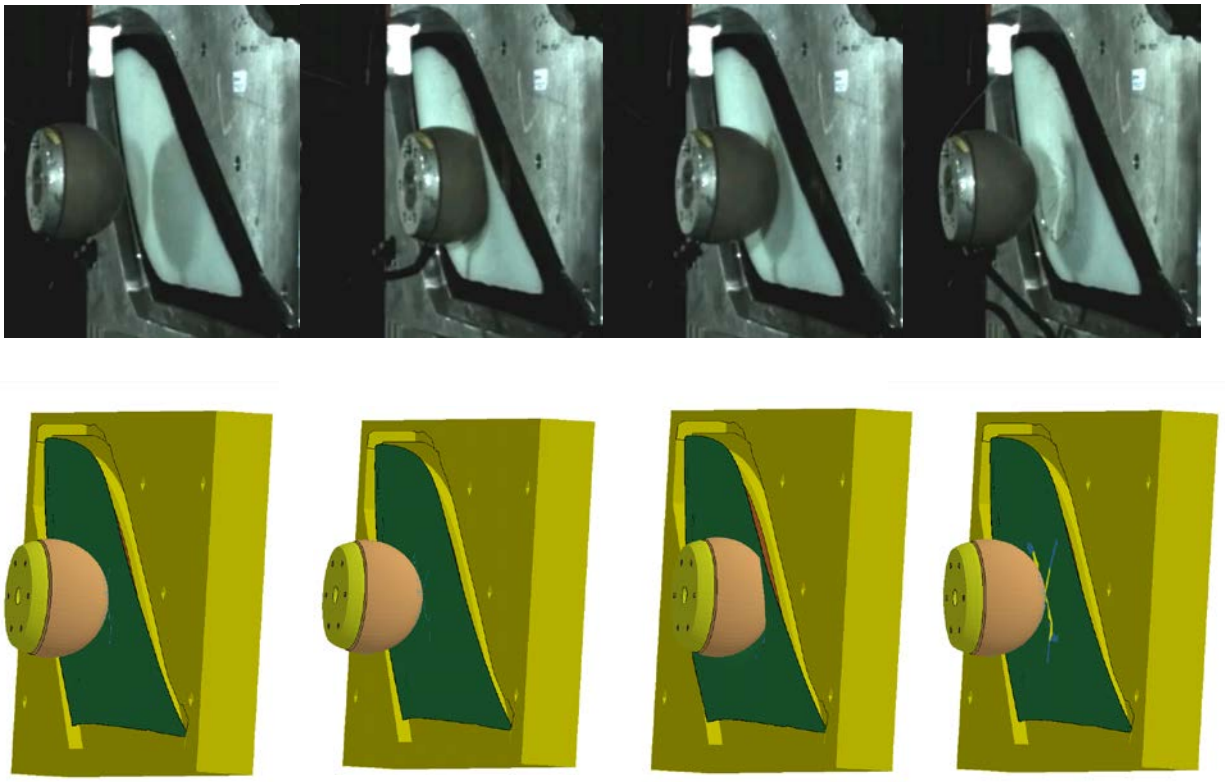

Figure 9 – Image series of the head impact test at 10 m/sand room temperature test compared to simulation results.

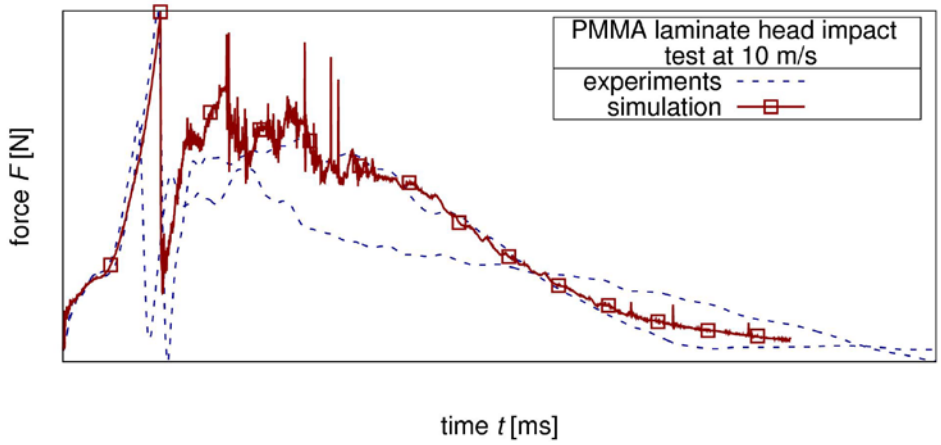

Figure 10 – Image series of the head impact test at 10 m/sand room temperature test compared to simulation results.

7 Summary and Outlook

The substitution of conventional glass products by amorphous polymeric structures bears a huge weight reduction consisting of poly(methyl methacrylate) (PMMA) and thermoplastic polyurethane (TPU) was investigated experimentally and numerically with regard to its impact behavior and applicability. Basic experiments with PMMA and TPU were used to identify the mechanical characteristics of the monolithic materials. Furthermore, PMMA-TPU-PMMA laminates were subjected to impact loadings at 5 m/s using dart impact tests. The principle behavior, characterized by a distinct post-breakage capacity, was examined. Based on the experimental basis, different material models for the Finite Element simulation are presented. These material models are capable to capture the temperature and time dependent behavior of the laminate. A final validation experiment, consisting of head-dummy impacts at 10m/s on automotive side windows, was conducted for PMMA and the laminate. The corresponding simulations showed very high agreement to experimental results and exhibited as reliable prediction tools for future developments. Further experimental and numerical studies as well as deeper discussion can be found in [13]. Investigation of the stochastics of failure in dependence on triaxiality and its influence in full car crash situations are topics of further research.

8 Literature

[1] Illinger, J., Lewis, R., Barr, D.: "Effect of Interlayer on Impact Resistance of Acrylic / Polycarbonate Laminates", Polymer Preprints vol. 16.1, 1975, pp. 545-550.

[2] Stenzler, J., Goulbourne, N.: "The effect of polyacrylate microstructure on the impact response of PMMA / PC multi-laminates", International Journal of Impact Engineering vol. 38.7, 2011, pp. 567-576.

[3] Antoine, G., Batra, R.: "Low speed impact of laminated polymethylmethacrylate / adhesive / polycarbonate plates", Composite Structures vol. 116.1, 2014, pp. 193-210

[4] Kolling, S., Alter, C., Rühl, A.: " Experimentelle und Numerische Untersuchungen von Windschutzscheiben unter stoßartiger Belastung zur Verbesserung des Fußgänger- und Insassenschutzes", Abschlussbericht BMBF Projekt 17N1111, 2015.

[5] Alter, C., Kolling, S., Schneider, J.: " Verhalten von Glas und Simulation des Nachbruchverhaltens von Verbundverglasung bei kurzzeitiger Beanspruchung", Abschlussbericht BMBF Projekt 17N1111, 2015.

[6] Kuntsche, J.: "Mechanisches Verhalten von Verbundglas unter zeitabhängiger Belastung und Explosionsbeanspruchung", PhD thesis, TU Darmstadt, Springer 2015.

[7] Hoess, W. et al.: "Transparent plastic composite", US Patent US20090226730 A1, 2009

[8] Hoess, W., Schmidt, A., Manis, A.: " Elastomer PMMA layered composites having improved properties", US Patent US20160101607 A1, 2016.

[9] Williams, M.L., Landel, R.F., Ferry, J.D.: The Temperature Dependence of Relaxation Mechanisms in Amorphous Polymers and Other Glass-forming Liquids. Journal of the American Chemical Society 77, 1955, pp. 3701.

[10] Pyttel, T., Liebertz, H., Cai, J.: "Failure criterion for laminated glass under impact loading and its application in finite element simulation", International Journal of Impact Engineering, vol. 38.4, pp. 252–263, 2011.

[11] Belytschko, T., Black, T.: "Elastic crack growth in finite elements with minimal remeshing", International Journal for Numerical Methods in Engineering vol. 45.5, pp. 601–620, 1999

[12] Lopez-Ruiz, D. et al. "CAE validation study of a side window impact using Plexiglas materials", 10th European LS-DYNA Users Conference, 2015.

[13] Rühl, A. "On the Time and Temperature Dependent Behaviour of Laminated Amorphous Polymers Subjected to Low-Velocity Impact", PhD thesis, TU Darmstadt, Springer, 2017